**Geomechanics and Engineering**, *Vol. 27, No. 3 (2021) 273-290*
https://doi.org/10.12989/gae.2021.27.3.273


# DEM modelling of retained backfill: Influence of particle shape for different stress paths and densities

Adlen Altunbas[1a], Behzad Soltanbeigi[2b] and Ozer Cinicioglu*[3]

[1]*Department of Civil Engineering, Medipol University, Istanbul, Turkey,*
[2]*Van Oord Dredging and Marine Contractors, Rotterdam, The Netherlands,*
[3]*Department of Civil Engineering, Bogazici University, Istanbul, Turkey*

*(Received July 14, 2020, Revised November 22, 2020, Accepted October 5, 2021)*

**Abstract.** This paper investigates the relative influences of backfill particle properties and imposed stress path on the response of retained granular assemblies. The characteristics considered are particle shape, backfill density, and gradation. For this purpose, Discrete Element Modelling (DEM) is employed to simulate the development of passive and active states in a cohesionless soil. Particle shape is assessed first through restraining the rotational freedoms of spherical particles (i.e. assigning rolling resistance), and the next by joining spherical particles (i.e. multisphere). The obtained results show that it is not possible to capture realistic response using a contact-independent rolling resistance model. Then, using backfill models composed of particles with various angularities, which are prepared at two alternative densities, backfill deformation towards passive and active states are simulated. Results are used to judge the relative weights of the influences of particle angularity, backfill density and gradation on back behaviour, employing both qualitative and quantitative methods. For densely packed clump particles varying particle angularity influences backfill density, shear band characteristics, geometries of the resulting failure wedges, and distribution of lateral backfill pressure. In addition, the effect of shape complexity is evaluated for packings with identical initial density, which are relatively loose. Overall, comparing the results from packings with different densities revealed the idea that particle shape effect is density and stress-path dependent.

**Keywords:** active state; density; Discrete Element Modelling (DEM); particle shape; passive state; retaining wall

## 1. Introduction

Retaining walls are constructed for all projects where grading and levelling of topography are required. This might involve road projects, building sites, waterfront and flood control facilities, or stabilization of the unstable ground. In all cases, the quality of retaining wall design is dependent on the extent of our understanding of backfill behaviour which is the major source of loading on the retaining structure. As for all engineering structures, the design must satisfy both ultimate and serviceability limit states. Ultimate limit states involve either an external or an internal stability problem. External stability is controlled by the soil, whereas internal stability depends on the structure. For both cases, the stresses that act on the retaining system must be determined. Lateral stresses imparted from a backfill are dependent on the mode of wall failure. If a retaining system is failing by moving away from the soil, limiting lateral stresses are referred to as active stresses. In case limit state is reached by wall moving towards backfill, limiting lateral stresses are passive stresses. Therefore, the calculation of lateral stresses at the limit states is central to retaining wall design. This requirement is first addressed by Coulomb (1776) and Rankine (1857).

Due to their inherent simplicity, lateral earth pressure theories developed by Coulomb (1776) and Rankine (1857) are still in wide use in engineering practice. Coulomb theory is an upper-bound solution and Rankine theory is a lower-bound solution. Both theories assume the slip plane within the backfill to be linear.

Early in the 20th century, experimental studies revealed that the slip line that develops in the backfill is not linear. Terzaghi (1943) suggested the log-spiral function to define the form of slip lines at the limit states. Even though the log spiral function results in more accurate lateral earth pressure estimations, it never became popular among design engineers due to its complexity. But, its real impact is to highlight the need for understanding the mechanisms that control the formation of slip bands within retained soils.

In the literature on the behaviour of retained backfills, mode of wall movement, interparticle cohesion and friction, interface friction and wall geometry are considered to be the major influences on the failure mechanism that develops in retained soils (Hanna and Al Khoury 2005, Nadukuru and Michalowski 2012, Niedostatkiewicz *et al.* 2011, Rechenmacher *et al.* 2011, Soltanbeigi *et al.* 2019, Tejchman *et al.* 2007, Toyosawa *et al.* 2006). Another major influence that is acknowledged especially in the last decades is grain shape. It is an established fact that grain shape influences engineering properties of granular assemblies, among which peak and critical state friction

*Corresponding author, Ph.D. Associate Professor
E-mail: ozer.cinicioglu@boun.edu.tr
[a] Ph.D., Assistant Professor
[b] Ph.D., R&D Engineer


http://www.techno-press.org/?journal=gae&subpage=7
ISSN: 2005-307X (Print), 2092-6219 (Online)

angles, permeability, compactibility, small-strain stiffness are the most prominent. Holubec and D'appolonia (1973), and later Holtz *et al*. (1981) argued that all engineering properties of soils are affected by particle shape and increasing grain angularity results in greater maximum void ratio, strength, and deformability in the case of cohesionless soils. Cho *et al.* (2006) determined empirical correlations between particle shape quantifiers and soil characteristics such as range of packing densities, stiffness, compressibility, and critical state parameters. Based on the empirical evidence, Cho *et al*. (2006) advocated the inclusion of particle shape determination in methods of soil classification.

Investigating the effect of particle shape on soil behaviour uncoupled from the influences of grain size, packing density and gradation is a difficult task facing researchers. There have been several experimental studies to understand the isolated influence of particle morphology. Holtz *et al*. (1981) asserted that particle size does not have any effect on the peak friction angle, as long as the tests are conducted at the same void ratio. Vangla and Latha (2015) recently supported this suggestion and argued that at the same void ratio, the particle size of sand does not influence peak shear strength when particle morphology is unchanging. On the other hand, Vangla and Latha (2015) observed that magnitudes of peak and ultimate friction angles, as well as dilatancy angles, are significantly affected by particle shape and gradation. Results obtained by Shin and Santamarina (2013), and later by Lim *et al.* (2012) reinforced this proposition by showing the influences of grain shape and gradation on friction and dilatancy angles. These studies presented several empirical relationships that correlate shape quantifiers with soil behaviour; however, it must be noted that the mechanism behind the empirically obtained results is still not completely understood (Rodriguez *et al.* 2013).

Attempts to investigate the influences of packing density, gradation and grain shape on the behaviour of retained soils utilized different methods, such as model tests (Alper Kamiloğlu and Sadoğlu 2019, Altunbas *et al*. 2017, Gezgin and Cinicioglu 2019, Keshavarz and Pooresmaeil 2016, Lee 2019, Niedostatkiewicz *et al*. 2011, Sancak and Cinicioglu 2020, Zheng *et al*. 2015, Zhuang *et al*. 2013), and numerical studies (Altunbas *et al*. 2019, Jiang *et al*. 2014, Widuliński *et al*. 2011). Among these, model tests provide the most realistic insight, however, owing to the difficulties in controlling and measuring the properties of models, they are not useful especially when the goal is to investigate the influences of micro-mechanical characteristics. Furthermore, with model tests, observing the uncoupled influences of grain characteristics on retained soil response is next to impossible. On the other hand, numerical methods, such as finite element and finite difference methods, allow the researcher direct control over model properties. But these continuum mechanics-based models cannot simulate the granular nature of soils. At this point, discrete element modelling (DEM) provides a powerful option as it allows modelling granular assemblies.

Discrete Element Method (DEM), developed by Cundall and Strack (1979), considers granular material as a system of distinct interacting bodies and provides insight into the granular response.

Widuliński *et al*. (2011) evaluated the capability of DEM to generate the pattern of shear zones under active and passive states. They considered various wall movements (i.e. horizontal translation, rotation about top and toe) and used spherical particles. Results are compared with both experimental (through X-rays and DIC analysis) and numerical (through FEM) approaches, and it is shown that DEM realistically predicts shear zone patterns.

Jiang *et al*. (2014) used DEM to investigate wall pressure distribution with respect to various types of wall movements. For this purpose, a contact model that incorporates a rolling resistance model is employed (the model hinders particle rotation to replicate the effect of particle interlocking). Accordingly, their study evaluated the dependency of bulk response on applied rolling resistance and argued that it is essential to consider rolling resistance to create realistic responses.

Zhao *et al.* 2017 studied the effect of particle angularity using (DEM) in which particles with different angularities are modelled using convex polyhedra. Simulating direct shear tests with these angular particles, (Zhao *et al.* 2017) stressed that angularity plays an important role in enhancing particle interlocking.

Khosravi *et al*. (2017) investigated the problem of a retaining wall under active translation numerically using the discrete element code, PFC2D. They used discs as individual soil particles and observed that, due to the lack of interlocking between the soil particles, lower internal friction angles are mobilized. Therefore, they recommended the use of clumped particles in simulations.

This study attempts to examine the influences of particle shape, gradation, density and stress path dependency on the behaviour of retained backfill soils. Accordingly, DEM models of backfill are simulated, in which the sought-after characteristics are varied. In these models, only those problems that involve lateral translation of vertical walls that retain level backfills are considered. The boundary conditions (e.g. wall geometry, backfill inclination and wall rotation) are not varied between models to better understand the dependence of failure mechanism on micro-scale backfill characteristics.

When developing DEM models, the usability of different options to model particle shape is considered and evaluated. Once the appropriate modelling methodology is determined, DEM models are prepared with certain characteristics to facilitate comparative consideration and understanding. For this purpose, in the next section, the numerical model and its specifications are described. Following, the considered methodology to post-process and interpret the DEM data is explained. Overall, this systematic study will allow an understanding of the underlying mechanism of particle-level interactions and their influence over the bulk response of the particle assemblies at various density and stress paths. The influence of particle shape over geometrical characteristics of shear bands is investigated with this study. The variations of geometrical characteristics of shear bands and lateral thrusts for different particle shapes are given for both active

and passive problems at different densities. The results are reported quantitatively for all shear bands' characteristics considered.

## 2. Methodology

### 2.1 DEM simulation

The initial step in DEM is to define the geometry of the system, where particles are free to overlap while they come into contact. This study considers the so-called soft contact approach, in which particles are assumed rigid for shape definition purpose and allowed to overlap during contact (elastic deformations define contact forces). A detailed description of the work process on DEM can be found in the literature (O'Sullivan 2011, Soltanbeigi *et al.* 2018). Calculations in DEM are based on Newton's second law and force-displacement law at the contacts. Force-displacement law relates particle-to-particle contact forces to particle displacements and vice versa. Total normal and shear forces acting on each particle are calculated at each time-step by taking into account both the contact and body forces acting on the particles. Newton's second law of motion is applied following the determination of contact forces. This way, accelerations, velocities and displacements of each element are calculated between two succeeding time steps.

Accordingly, for particle $i$, the equation of motion is given by Eq. (1):

$$m_i (d^2x_i/dt^2)=f_i+m_ig \quad (1)$$

where $m_i$ is mass of the particle, $t$ is time, $x_i$ is particle's position, $g$ is gravitational acceleration and $f_i$ is the total force acting on the particle at contacts and defined in Eq. (2):

$$f_i=\Sigma f_i^c \quad (2)$$

where, $f_i^c$ is the individual contact force acting on particles. The rotational motion equation for particle $i$ is given by:

$$\text{Ii } (d\omega i/dt)=\text{Ti} \quad (3)$$

where $I_i$ is the moment of inertia for particle $i$, $\omega_i$ is angular velocity and $T_i$ is the total torque acting on it, which is defined by Eq. (4):

$$T_i = \sum_{i=1}^{Nc} l_i^c \times f_i^c \quad (4)$$

where $l_i$ is the branch vector of particle $i$, defined as:

$$l_i=r_i-r_j \quad (5)$$

The theory of DEM and its work process for calculating the position and force for individual particles are available in the literature (O'Sullivan 2011) and will not be repeated here.

### 2.2 Simulating the mechanical effect of particle morphology in DEM

Mechanical behaviours of granular assemblies are dependent on the interactions between individual particles of which they are composed. As expected, the nature and magnitude of these interactions are dependent first on the external boundary conditions, second on internal material properties. For the majority of geotechnical engineering problems where particle crushing is absent, single-particle properties dominate and control the overall response of the soil sample. It is known that particle morphology influences the motion of the particles, which leads to change in the contact force network, and thus stress distribution for the granular assembly. Therefore, to develop realistic DEM models, it is necessary to simulate the influence of particle shape.

However, defining the particle shape for non-spherical particles in DEM simulations is computationally demanding. In order to simulate the mechanical effect of particle shape without bearing the additional computational cost, a modelling option called rolling resistance is available in DEM (Ai *et al*. 2011, Iwashita and Oda 1998, Jiang *et al.* 2014). There are several rolling resistance models available in the literature and they are all designed to simulate the effects of non-spherical shape by restraining rotations of spherical particles. In this study, first, the suitability of using contact-independent rolling resistance to simulate particle shape effect will be investigated. That is why in the following section, the rolling resistance modelling options will be summarized, followed by an explanation for particle shape definition and quantification in DEM.

#### 2.2.1 Rolling resistance model

According to Ai *et al*. (2011) the available rolling resistance models can be classified into four categories:

a) Directional constant torque models: In this category, a constant torque is calculated and applied to particles in contact, which is independent of rotational velocity magnitude (Zhou *et al*. 1999). The general form of the equation for calculating torque is:

$$M_r = -\mu_r R^* F_n \omega_{rel} \quad (6)$$

where, $M_r$ is the torque, $\mu_r$ is the unitless rolling coefficient, $R^*$ is the equivalent radius, $F_n$ is the normal force magnitude at contact, and $\omega_{rel}$ is the relative rotation velocity.

b) Viscous models: In such models, angular velocities of particles directly influence the magnitude of calculated torque. A model from this category is proposed by Zhou *et al*. (1999):

$$M_r = -\mu_r R_r F_n(\omega_i r_i - \omega_j r_j) \quad (7)$$

where, $r$ is particle radius and $\omega$ is the rotational velocity vector.

c) Elastic-plastic spring-dashpot models: Torque in this model is composed of two parts: mechanical spring torque and viscous damping torque (Iwashita and Oda 1998, Jiang *et al*. 2005).

d) Contact-independent models: In this model, obtained torque is independent of relative rotation or rotational velocity of a pair of particles in contact. Instead, torque is dependent on the total rotation or rotational velocity of a particle (Bardet and Huang 1992, Sakaguchi *et al.* 1993).

Table 1 Particle shape properties

| Properties | M1 | M2 | M3 | M4 | M5 | M6 | M7 |
|---|---|---|---|---|---|---|---|
| Particle Shape | 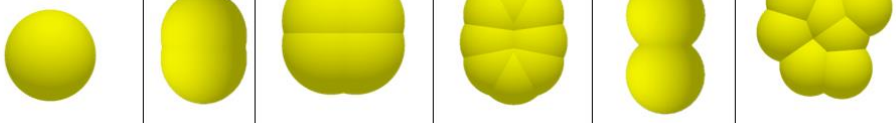 | | | | | | |
| Discretisation | Sphere | | 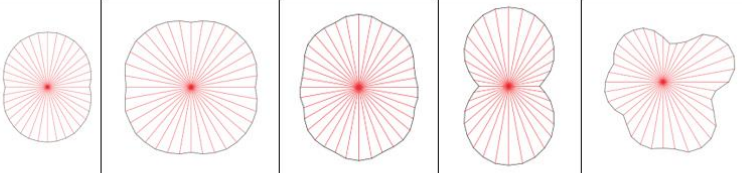 | | | | |
| Angularity Factor (*Af*) | 0 | 0 | 2.41 | 3.44 | 4.6 | 18.6 | 19.3 |
| Solid Fraction * (*Sf*) | 0.654 | 0.656 | 0.712 | 0.732 | 0.729 | 0.689 | 0.687 |

* At dense case

This study considers the default rolling resistance model implemented in EDEM, which incorporates the radius ($R_i$) and unit rotational velocity vector $\hat{\omega}_i$ of individual particle into torque calculation:

$$M_r = -\mu_r R_r F_n(\omega_i r_i - \omega_j r_j) \quad (8)$$

In this model, applied torque reduces the rotational velocity of particles in all conditions. According to (Ai *et al.* 2011) any model in the form of Eq. 8 (depending on how $\omega$ is considered in the model) can be categorised as, either a directional constant torque model or a contact-independent model. Since torque calculated using Eq. 8 is independent of relative rotation or rotational velocity of a pair of particles in contact, this model can be categorized as a contact-independent model (Type D).

### 2.2.2 Definition of particle shape

Sukumaran and Ashmawy (2001) proposed a new method for quantifying particle shape that provides angularity factor using an image analyser. This new method uses particle's two-dimensional projection to characterise shape and angularity. Normalized angularity factor (*AF*) is obtained by:

$$AF = \frac{\sum_{i=1}^{N}(\beta_{i\ particle} - 180)^2 - (360^2/N)}{3 \times (180)^2 - (360^2/N)} \times 100\% \quad (9)$$

where, $N$ is the sampling interval, $\beta_i$ is each of the internal angles of the particle. In this study, $N$ is chosen to be 10 degrees. With Eq. (9), *AF* of a sphere is 0%, whereas *AF* is 100% for the most-angular particle that is possible.

Table 1 summarizes particles defined in this study and their respective geometries, angularity factors and solid fractions. In Table 1, M1 and M2 are both spherical particles, where M1 is representing a mono-disperse and M2 is representing a poly-disperse system. The polydisperse granular system M2 consists of spherical particles with a mean diameter that is equal to M1. The polydispersity is achieved by a normal distribution with a standard deviation of 0.2.

The equivalent diameters of particles in all models are approximately equal to 5mm, which is equal to the diameter of M1 particles. The equivalent diameter ($d_{eq}$) of a particle is the diameter of a sphere of equal volume. On the other hand, solid fractions of the packings are obtained as the ratio of the total volume of particles to the volume of the entire DEM model box.

### 2.3 The numerical model

A cohesionless retained backfill that deforms under plane strain is modelled using a three-dimensional DEM set up, as shown in Fig. 1. This is achieved by defining models that utilize periodic boundary conditions (in *y* axis, see Fig. 1).

In DEM simulations periodic boundaries can be used to reduce computational burden and to prevent adverse boundary effects. The periodic boundary is defined by a periodic cell that is surrounded by identical copies of itself (O'Sullivan 2011). The length of the wall between two periodic boundaries is 20 mm (see Fig. 1). Additionally, generated particles are three-dimensional (either single spheres or overlapping spheres).

The retaining wall is vertical and has a planar rough surface. Retained backfill is horizontal and in level with the top of the model wall. The model wall can translate either towards or away from the backfill, ultimately resulting in either passive failure or active failure, respectively. Furthermore, the adverse influence of the bottom boundary is minimized by considering a layer of particles below the retaining wall.

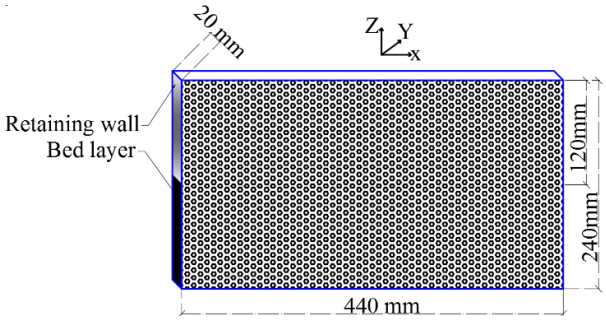


Fig. 1 The geometry of DEM model

Table 2 DEM material properties, Bono and McDowell (2014)

| Parameter | Unit | Value |
|---|---|---|
| Density | kg/m3 | 2650 |
| Sliding friction ($\mu_s$) | - | 0 - 0.68 |
| Interface friction ($\delta$) | - | 0.45 |
| Poisson ratio | - | 0.25 |
| Restitution coefficient | - | 0.8 |
| Shear modulus | Pa | 2.8e10 |
| DEM time-step | S | 2e-6 |

The properties of particles in this layer are the same as those in the upper part of the backfill and the depth of this zone is equal to the height of the retaining wall (Fig. 1). Table 2 summarizes the properties DEM model that is common in all simulations. In modelling the backfill, typical values for quartz sand are used, as defined by Bono and McDowell (2014). DEM simulations and analyses were conducted using EDEM® 2017 bulk material simulation software provided by DEM Solutions Ltd., Edinburgh, Scotland, UK.

In all simulations, the wall is translating with a low constant speed (2 mm/s in passive case and 1 mm/s in active case) to ensure the quasi-static flow of the particulate system (Soltanbeigi *et al.* 2016). The particle data is saved with a frequency of 200 Hz.

Regarding backfill density, two different model types are used in this study; models with densest possible backfills and models with backfills prepared at a common target density.

In order to prepare the models at the densest possible state, rolling and sliding frictions are set to zero at the filling stage.

Subsequently, air-pluviated granular assembly is levelled by removing the particles above the top of the wall. Then, before moving the wall model, sliding friction values for particle-to-particle and particle-to-geometry contacts are changed to 0.68 and 0.45, respectively. In cases when the model utilizes rolling resistance, model-specific rolling friction is assigned to all particles. After assigning friction parameters, simulation is continued for an additional 0.5 seconds while the granular assembly remained at rest for the system to stabilize.

However, if the goal is to prepare models at a target density, sliding friction is tuned during the pluviation stage

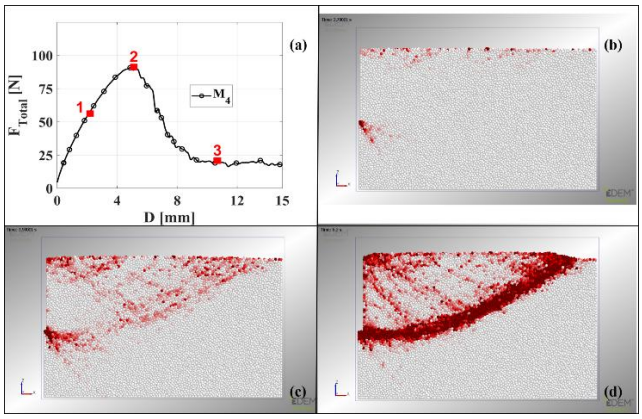


Fig. 2 Influence of wall movement on the magnitudes and spatial distribution of cumulative particle rotations for dense M4 model a) total force acting on the retaining wall, b) cumulative rotation distribution at D=2.5mm c) D=5mm d) D=10mm.

to a value that will provide a backfill with the target solid fraction. The target solid fraction for those models with common backfill density is chosen as 0.655; this value is the average of the solid fractions of the models with mono- and poly-disperse spherical particles when they are at their densest states (Table 1).

After the simulations are completed, the results are investigated both qualitatively and quantitatively. Qualitative work is done using the visual outputs of the models. A quantitative comparison is done considering the following main points; calculation of particles' cumulative rotations, total force acting on the retaining wall, determination of the emerging failure surface's geometry, position, inclination, and thickness.

### *2.3.1 Cumulative rotation determination*

Oda and Kazama (1998) closely observed the particle rotation in a sheared particle assembly and pointed out that maximum particle rotations are distinguished within shear bands. Accordingly, the spatial distribution of the magnitudes of cumulative rotations of single particles can be used to determine the positions of localised deformations. Following, localised deformations can be used to identify the position and the geometry of the failure surface.

The cumulative rotation $\theta_i$ and its magnitude $\theta_i$, for each particle *i*, is calculated using Eq. 10 and then recorded for all tests:

where, $\boldsymbol{\omega_i}$ is the angular velocity of particle *i* and $N_p$ is the number of particles in the system.

$$\boldsymbol{\theta_i}(t) = \frac{1}{2\pi}\int_0^t \boldsymbol{\omega_i} d\tau \ , \quad \theta_i = \left|\left|\boldsymbol{\theta_i}\right|\right| \ , \quad i = \overline{1, N_p} \quad (10)$$

An example of the variation of the spatial distributions and the magnitudes of cumulative particle rotations as functions of wall translation is shown in Fig. 2. Fig. 2 also illustrates the dependence of the thrust exerted on the wall on the backfill response. The results presented in Fig. 2 are obtained from the simulation with M4 particles. Fig. 2a presents the variation of total force exerted on the wall

($F_{TOTAL}$) with respect to wall translation ($D$). As illustrated in Fig. 2(a), $F_{TOTAL}$ increases until the peak resistance is mobilized at $D$=5mm, after which strain-softening starts until $F_{TOTAL}$ drops to critical state at $D$=10mm. Cumulative particle rotations and their distributions are obtained for three different wall displacements; these are $D$=2.5mm, $D$=5mm, and $D$=10mm as shown in Figs. 2(b)-(c) and Fig. 2(d), respectively. Evidently, Fig. 2(b) shows the distributions of cumulative rotations prior to the mobilization of peak resistance within the backfill and at this stage, there is not a continuous shear band yet. However, at the second point (Fig. 2(c)), where the peak strength is recorded, it is obvious that the failure wedge is fully formed. Finally, in Fig. 2(d) corresponding to $D$=10mm, backfill soil reached critical state and a more distinct failure wedge is observed. It is clear that the failure wedges are curvilinear, which is in agreement with experimental observations (Niedostatkiewicz *et al*. 2011, Soltanbeigi *et al.* 2020). Furthermore, the position of the shear band does not vary throughout wall translation as previously shown by the experimental results of Soltanbeigi *et al.* (2019).

### 2.3.2 Determination of failure surface geometry

Identified failure surfaces can be quantified by establishing a coordinate system as shown in Fig. 3. The origin of the coordinate system coincides with the bottom of the model wall. All distances are made dimensionless by normalizing the axes with model wall height ($H_w$). Measurements of coordinates of points along failure surfaces for active and passive cases are depicted in Fig. 3. In this respect, coordinates of the points along the failure surfaces are identified as either $B$ (away from the model wall) or $H$ (parallel to the model wall) as shown in Fig. 3. Note that the greatest distance between the failure surface and the retaining wall is defined by $B_f$. All measurements are made with respect to the position of the wall prior to any displacement. Additionally, Fig. 3 illustrates the method by which shear band inclination (α) is measured.

A visual interpretation of the cumulative rotation change, along with the shear bands, can be obtained by utilizing intensity profiles. For this purpose, RGB images are converted to greyscale using MATLAB. In grayscale, the lowest possible intensity is zero (black), and the highest is 255 (white). In the grayscale image, brighter particles visually represent low cumulative rotation, whereas, darker particles define high cumulative rotation. The variations of cumulative rotation along three cross-sections (A-A, B-B, and C-C) are quantified using the intensity profile tool (Image Processing tool in MATLAB), as shown in Fig. 4 a and b. Cross-sections are chosen at regular intervals along with the main shear band.

It must be noted that the determination of shear band thickness ($t_s$) can be challenging owing to the problems associated with the identification of shear band boundaries (Soltanbeigi *et al*. 2019). Soltanbeigi *et al*. (2019) proposed a $t_s$ measuring method that is applicable for all problems, independent of the boundary conditions. In this approach, tangents are applied to two tails of the intensity profile, where the rates of intensity changes are almost constant. The boundaries of the shear band correspond to the points

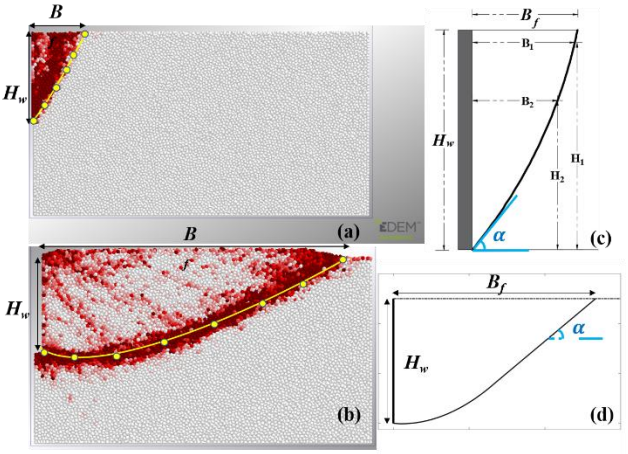


Fig. 3 Determination of failure surface geometry and locating the outer boundary of a) active and b) passive failure surfaces, and the corresponding digitized results c) active d) passive

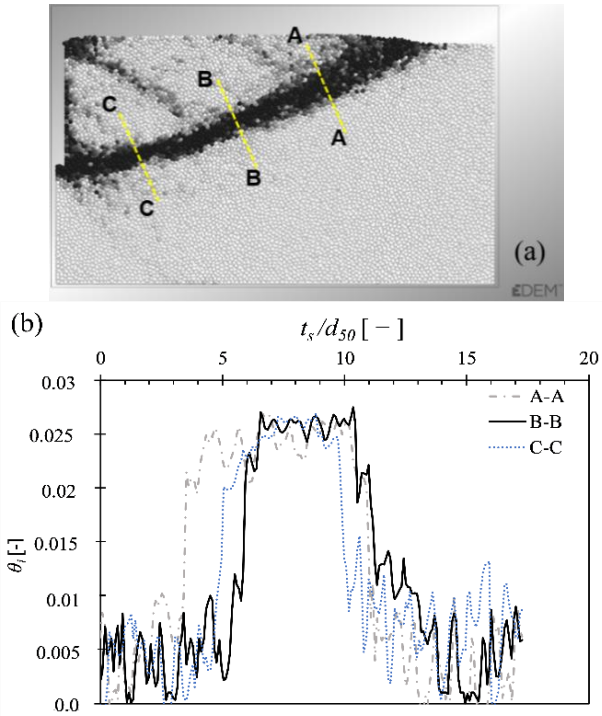


Fig. 4 Example for determining shear band thickness a) location of three cross-sections b) intensity profiles.

where the tangents from tails intersect on either side. Soltanbeigi *et al*. (2019) referred to this approach as *Method II*, where shear band thickness is defined as the distance between two boundaries. In this study, using *Method II*, the shear band thickness is determined for all three cross-sections and the obtained values are averaged ($t_s$). Determined shear band thicknesses are all normalized with equivalent grain diameter ($t_s$ / $d_{eq}$).

### 2.3.3 Validation of the numerical model

The purpose of this work is to conduct a parametric modelling study using DEM to reveal the influences of particle-scale granular properties on bulk backfill response.

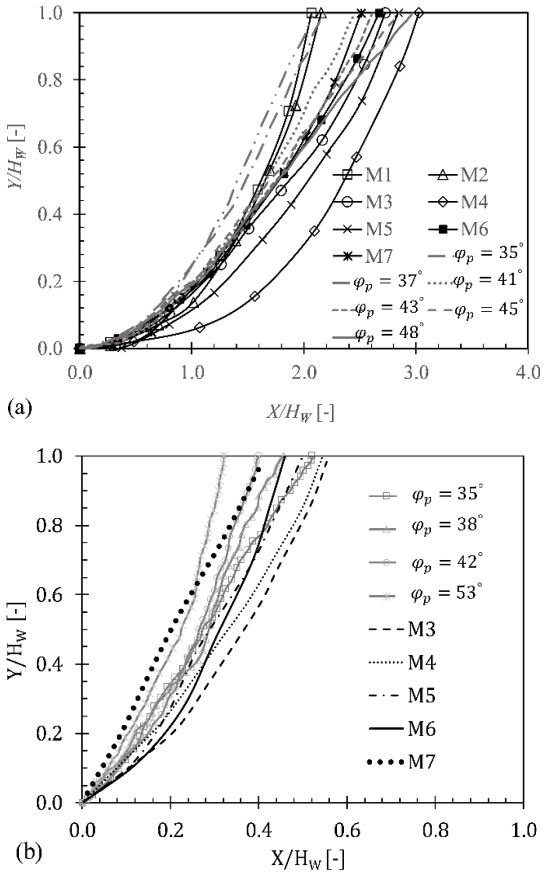


Fig. 5 Comparison of failure surfaces from physical tests and DEM models a) passive tests (experimental data from Soltanbeigi *et al*. 2020) b) active tests (experimental data from Altunbas *et al*. 2017).

However, it is necessary to show whether the outputs of models with the assigned parameters lead to realistic responses. For this purpose, the results of DEM models are compared with those of similar experimental studies available in the literature. The details of the experimental models against which the results of this study are compared, can be found in Soltanbeigi *et al.* (2020) for passive models and in Altunbas *et al*. 2017 for active models. The outcome of the comparison is presented in Fig. 5. Apparently, DEM models produce realistic failure surfaces for both passive and active simulations.

## 3. Results and discussions

As explained previously, this study explores the influence of particle shape on backfill behaviour at different density states and stress paths. For this purpose, the first step is to examine the suitability of using rolling resistance as a substitute for angular particles. This will be attempted a Type D rolling resistance model that is the default in EDEM.

Following, the influence of particle shape on backfill response is inspected for different packing densities (i.e. densest possible versus same density) and stress paths (passive versus active). Densest possible condition is a property unique to granular assembly and can be considered as a reference state. On the other hand, models can be prepared at the same density, defining a predetermined density as a "reference density". Models prepared at the densest state and models prepared at the reference density are subjected to two possible different modes of deformation; active and passive.

### 3.1 Influence of rolling resistance

In this section, the suitability of using the default rolling resistance model in EDEM to simulate the effects of particle shapes is tested. As mentioned in Section 2.2.1., the default rolling resistance model in EDEM is considered as Type D (i.e. contact independent model). In literature, it is noticed that the suitability of the default rolling resistance model in EDEM is problem-dependent (Gezgin *et al.* 2020, Gezgin *et al.* 2021, Soltanbeigi, 2019). Thus, in this study, the capability of the default rolling resistance model in EDEM is evaluated for retaining wall problems. For this purpose, models with spherical particles are prepared at densest possible states as described in the numerical model section, while rolling resistance is off. Then, before the initiation of wall movement, the rolling resistance is applied to the granular assembly. The value of rolling friction varied between models to assess the sensitivity of bulk response to this micro-scale parameter (i.e. $\mu_r$=0, 0.01, 0.1, 0.2, and 0.5). After assigning rolling friction, simulation is continued for an additional 0.5 seconds while the granular assembly remained at rest for the system to stabilize.

Experimental studies show that soils with more angular particles have higher shearing resistances, and accordingly greater internal friction angles (Alshibli and Cil 2018, Cho *et al*. 2006, Shin and Santamarina 2013). It is a well-established fact that backfills with greater friction angles produce larger failure wedges at the passive limit state. This behaviour was first described by Coulomb (1776) and later corroborated by other researchers (Altunbas *et al*. 2017, Niedostatkiewicz *et al*. 2011). Accordingly, the point where the failure surface intersects with the ground surface is farther away from the retaining wall for backfills with more angular particles. Since it is assumed that rolling resistance will simulate the effect of angularity, it is expected that models with higher defined rolling resistances would produce larger failure wedges at the passive state; in other words, they will behave as though they are composed of more angular particles. Failure surfaces, obtained from models in which Type D rolling resistance is the only distinguishing factor, are shown in Fig. 6. When the results in Fig. 6 are examined, it is noticed the obtained results contradict the well-defined mechanical response of granular materials. Therefore, Type D rolling resistance fails to simulate the effect of particle angularity.

Additionally, variations of $F_{TOTAL}$ with $D$ are examined (Fig. 7). It is evident in Fig. 7 that the consideration of Type D rolling resistance results in lower total force, which is consistent with the results given in Fig. 6. However, this outcome contradicts the well-established granular response. This disparity with the expected mechanical response can be justified by the fact that the torque calculated in Type D rolling resistance is directly dependent on the magnitude of normal contact force (Eq. 8).

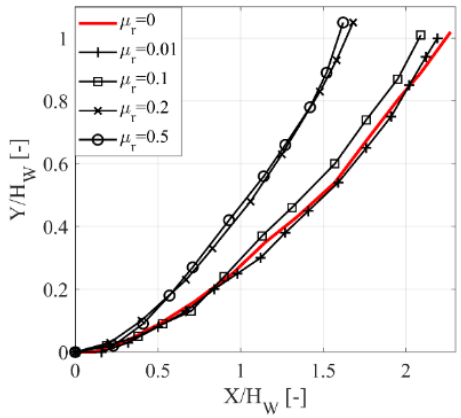


Fig. 6 Determination of passive failure surfaces in the presence of Type D rolling resistance

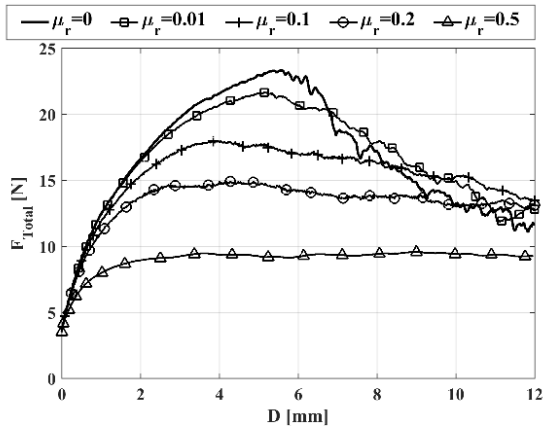


Fig. 7 Comparison of $F_{TOTAL}$-$D$ relationships obtained from DEM models with different magnitudes of Type D rolling resistances.

The mechanically unsound response obtained when the default EDEM rolling resistance model is utilized is because Type D rolling resistance model calculates incorrect torque values for this specific problem. However, in case of the angle of repose and silo discharge problems, for which external loads are absent, Type D rolling resistance model yields satisfactory results (Soltanbeigi 2019). This is a consequence of the way the torque values in Type D models are obtained; here torque is calculated linearly and without a limiting threshold based on normal contact force, coefficient of rolling friction, the radius of particle and unit angular velocity vector. This way the problem dependency of this model can be justified based on differences in the stress states of the problems investigated. As mentioned, the angle of repose test is a free-flowing case, whereas in direct shear (Soltanbeigi 2019), pile penetration (Gezgin *et al.* 2020) and passive backfill failure problems external loads are applied to the system. Clearly, Type D rolling resistance model is not suitable for problems that involve imposed loads and/or deformations.

Based on the obtained results, it is concluded that the default rolling resistance model in EDEM fails to simulate a realistic response for the problem considered, and therefore rolling resistance is no longer considered in the DEM models of this study.

### *3.2 Influence of particle shape on densely packed backfill response*

Densest possible configuration is an inherent property of a granular assembly. Depending on the shapes of particles that constitute backfill, the resulting solid fraction ($SF$) at the densest state will be different. Therefore, densest packing provides a natural state to observe the effect of particle shape on backfill response. In this section, behaviour of backfills composed of different shaped particles, prepared at their densest states, are investigated for passive and active states.

#### *3.2.1 Passive state for densely packed models*

In this section, the influence of particle shape and polydispersity on backfill response is investigated when a model wall moves laterally towards it, ultimately simulating passive failure. To understand the influence of particle shape on behaviour, clumped particles corresponding to different levels of angularity are used (Table 1). Seven DEM models, each with a different particle shape that is defined in Table 1, are prepared.

Spatial distributions of cumulative rotations are obtained at the instance where the total force on the wall reaches steady-state condition (i.e. critical state – point 3 in Fig. 2). Distributions of cumulative rotation magnitude ($\theta_i$) in these seven models are all shown in Fig. 8.

Note that by comparing M1 and M2, size distribution is considered for spherical particles. For a backfill made up of mono-sized spherical particles (M1), $\theta_i$ is distributed almost over the entire failure wedge with the highest concentration adjacent to the rigid boundaries (Fig. 8(a)). Additionally, for the system with poly-disperse spherical particles (M2), it can be observed that the overall distribution of $\theta_i$ is similar to that of M1 (Fig. 8(b)). However, when compared to M1 model, particles in M2 model undergo a relatively lower amount of rotation. This can be attributed to the fact that within a poly-disperse system, the number of contacts is higher. A higher number of contacts results in further suppression of particles' rotational freedom, which is in agreement with observations of Wiącek and Molenda (2014).

It must be noted that the models used for Fig. 8 do not include rolling resistance. In the absence of rolling resistance, spherical particles cannot produce distinct shear bands. This shortcoming is observed first by Iwashita and Oda (1998) and later were corroborated by other researchers (Zhou *et al.* 1999, Jiang *et al.* 2005, Tang *et al.* 2016). Zhuang *et al.* (2014) conducted experiments on sands and glass beads to determine the influence of particle shape on shear band characteristics. They observed wider and more diffuse shear bands for glass beads. For an assembly composed of spheres, the boundaries of the shear band are rather unclear, irrespective of the system being mono or poly-disperse. Under such circumstances, spherical particles have excessive rotational freedom, which leads to disperse distribution of cumulative rotations (i.e. deformations are less likely to localize). Accordingly, in this study, the diffuse nature of the shear bands shown in Figs. 8(a)-8(b) obtained from models composed of spherical particles without applied rolling resistance confirm these observations.

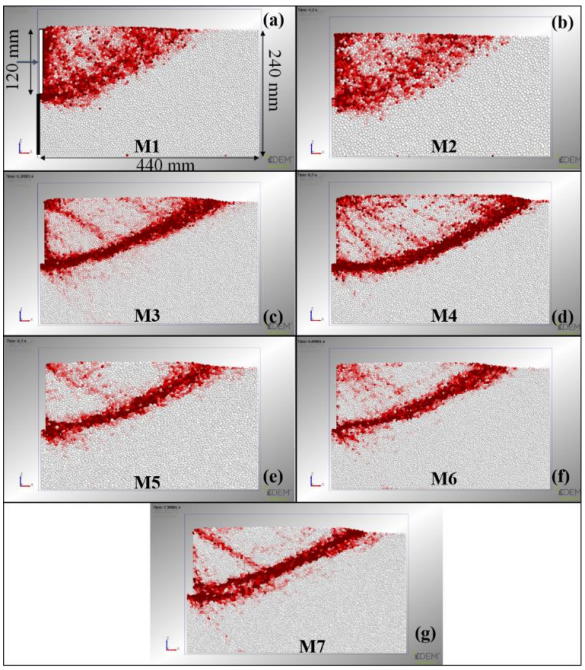


Fig. 8 Distributions of cumulative rotation magnitude ($\theta_i$) in passive tests with densely packed granular systems

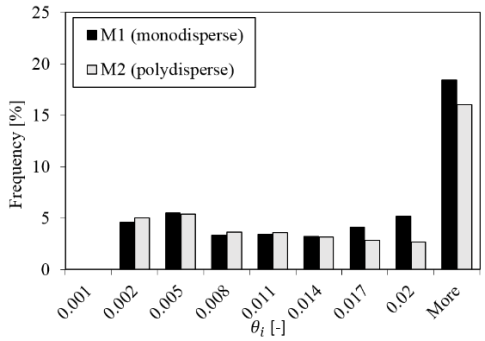


Fig. 9 Comparison of cumulative rotation magnitudes for the particles of M1 and M2 models in passive tests with densely packed granular systems (data are obtained at wall movement of 4mm)

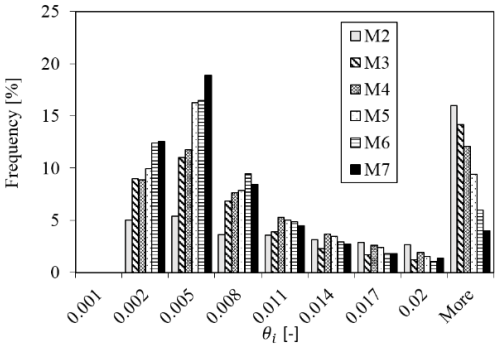


Fig. 10 Comparison of cumulative rotation magnitudes for particles with various angularity factors, passive case with initially dense packing (data are obtained at the steady state)

On the other hand, for assemblies made up of non-spherical particles, independent of angularity factor (*AF*), a distinct shear band emerges. Despite relative resemblances of these shear bands, it must be noted that their geometrical characteristics (e.g., thickness, curvature, and position), are not alike. This is an indication of the direct dependency of shear band characteristics on particle shape. When the results of DEM models with clumped particles are examined, it is noted that the main shear bands are distinct, and they connect the toe of the wall to the free ground surface. The main shear band serves as the demarcation line between the failure wedge and the rest of the backfill. There is also a secondary shear band that initiates at the top of the wall and extends to connect to the main shear band roughly at the midsection (e.g. Fig. 8(c)). This is congruent with the observation reported by Niedostatkiewicz *et al.* (2011).

To compare obtained cumulative rotation distributions quantitatively, the rotation data for all particles are extracted at instances of steady-state (corresponds to point 3 in Fig. 2). It must be noted that the extracted data is sorted according to the magnitudes of $\theta_i$. Then the particles undergoing similar amounts of rotations are grouped. These groups are shown in Fig. 9. Moreover, particles with $\theta_i \leq 0.001$ are excluded from the analyses (as these particles are assumed to be nearly stationary).

Frequencies of different amounts of rotations among all particles based on the selected groups are shown Fig. 9. Here, frequency is determined by dividing the associated number of particles by the total number of particles in each bin. Initially, in order to understand the influence of particle size distribution on cumulative distribution, the results of M1 and M2 models are compared in Fig. 9. It is clear that despite very small differences (i.e. M2 particles present less rotation), the rotational responses are similar. Next, the results for non-spherical particles are presented in Fig. 10, along with the results of M2 model. Here, results of M1 model are left out since they are the same as M2. Fig. 10 shows that for the passive failure of densely packed granular assemblies, increasing particle angularity results in greater restraint on particle rotation. In other words, models composed of more angular particles show higher frequencies in smaller rotation magnitudes.

Obvious in Fig. 10, frequency of particles with $\theta_i >$ 0.02 decreases with the increase in angularity. Combined with the observation of the visual results presented in Fig. 8, it can also be said that shear bands concentrate into narrower zones in cases when the particles are more angular, thereby decreasing the possible number of particles that experience large amounts of cumulative rotation.

To examine the influence of particle shape on generated shear bands, geometrical characteristics of the bands are evaluated. These characteristics include failure wedge geometries, shear band thicknesses and inclinations. Quantified failure wedge geometries are presented in Fig. 11. As expected, DEM models with spherical particles (M1 and M2) produce the smallest failure wedges (i.e. shorter $B_f$ distances), owing to their smaller shear resistances as explained in the previous sections.

However, when Fig. 11 is examined it is noticed that failure surface geometries are not simply following the increase in *AF*. Then, as an additional influence on shear band geometry, the impact of the solid fraction (*SF*) is

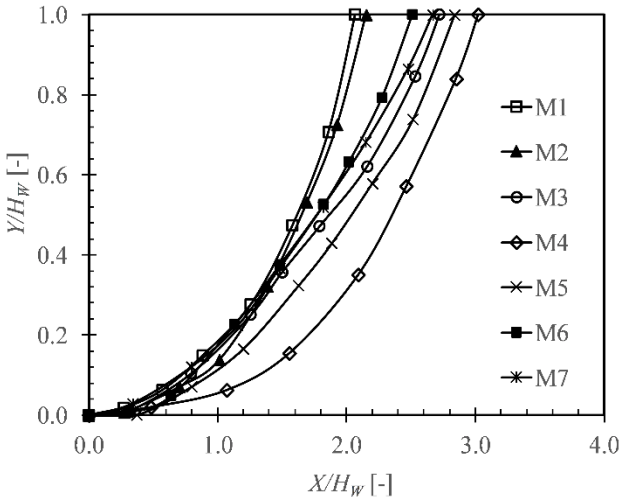


Fig. 11 Failure surface geometries for the densely packed particles with various shapes (passive state)

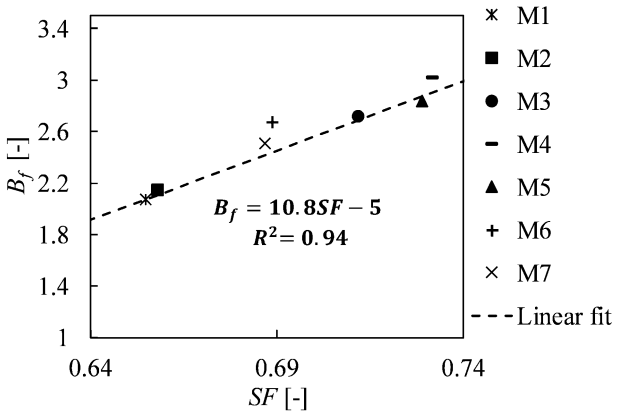


Fig. 12 Relationship between $B_f$ and $SF$ for densely packed granular assemblies at passive state

investigated. This is done by plotting $B_f$ versus $SF$ as shown in Fig. 12. When Figs. 11-12 are examined, it can be noticed that the presence of polydispersity marginally influences failure surface geometry, since M2 has a slightly larger wedge with respect to M1. Yet for the non-spherical particles, the first impression is that failure surfaces encompass larger areas as $AF$ increases. However, the results indicate that the largest failure wedge area is produced by M4 which has the third-highest $AF$ value with 3.44.

This can be justified by the fact that M4 has the largest packing density ($SF$=0.732). Additionally, with a slightly smaller packing density, M5 (SF =0.729, AF=4.6) yields the second-largest failure wedge. Despite having the smallest angularity factor among all models, $B_f$ distance for M3 ($SF$=0.712, $AF$=2.41) is longer than both M6 and M7. Although M6 and M7 have the largest $AF$ values with almost identical solid fractions, their passive failure surfaces are smaller than other models' with lower AF values (except spherical particles). Overall, the results suggest that particle shape and packing density have coupled influences over failure surface geometry of densely packed granular assemblies. Clearly, failure surface geometry is highly dependent on solid fraction for densely packed backfills, whereas angularity factor has minimal effect.

As explained in the methodology section, other considered geometrical characteristics of shear bands are thickness and inclination. It is known from available studies in literature that shear band thickness and its inclination for granular materials depend on several factors as: the average grain size, shape, relative density, stress state, stress-path and boundary conditions (Soltanbeigi *et al*. 2019, Widuliński *et al*. 2011, Jiang *et al*. 2014, Niedostatkiewicz *et al*. 2011, Nübel 2002, Nitka *et al*. 2015).

Respectively, variations of shear band thickness and inclination with angularity are shown in Figs. 13(a)-(b). Apparently, for densely packed passive models, $t_s$ / $d_{eq}$ reduces with increasing $AF$. Evidently, available results imply that the influence of $AF$ saturates after a certain threshold. On the other hand, a trend similar to $t_s$ / $d_{eq}$ – $AF$ is observed for $\alpha$ – $AF$, as given in Fig. 13 (b).

These results are expected as it is an established fact that both shear band thickness and its inclination are inversely proportional to the magnitude of dilation angle (Altunbas *et al*. 2017, Soltanbeigi *et al*. 2019, Tian *et al.* 2020). When all else is constant, increasing grain angularity enhances the tendency for dilation in a granular medium. Accordingly, the results are shown in Figs. 13(a)-(b) conform to this expected mechanical response.

When compared with the results of similar studies in literature, it is seen that the magnitudes of $t_s$ and $\alpha$ are comparable. For example, Widuliński *et al*. (2011) and Jiang *et al*. (2014) used DEM to simulate passive retaining wall failure. In these works, spherical particles with restrained rotations (i.e. Type C rolling resistance model) are used, yielding shear band thicknesses ranging between seven and eight mean particle diameters. Additionally, magnitudes of $\alpha$ agree with the results of similar studies (Jiang *et al*. 2014, Soltanbeigi *et al*. 2020). However, for shear bands that emerge at passive and active states, the influences of particle shape on $t_s$ and $\alpha$ are examined with this study.

The total forces ($F_{TOTAL}$) exerted on the wall are calculated by summing all individual particle-wall contact forces. Variations of $F_{TOTAL}$ with $D$ are determined and presented in Fig. 14 for the passive tests with dense packings. It is clear that models M1 and M2 that are composed of spherical particles, for which no rolling resistance is applied, exert the lowest $F_{TOTAL}$ over the entire movement of the wall. However, there is a significant increase in $F_{TOTAL}$ with an increase in $AF$. The model with the highest angularity factor, M7, provides the largest resistance against wall movement. Presented results in Fig. 14 agree with the underlying mechanics of the problem, according to which backfills with greater frictional resistances produce greater passive thrusts.

Meanwhile, definitive correlations can be found neither between peak $F_{TOTAL}$ values and angularity nor between peak $F_{TOTAL}$ values and packing density.

Evident in Figs. 11-14, failure wedge size is not the only factor that controls $F_{TOTAL}$. For instance, size of the failure wedge is smaller in M7 than in M4 or M5 (Fig. 12) but

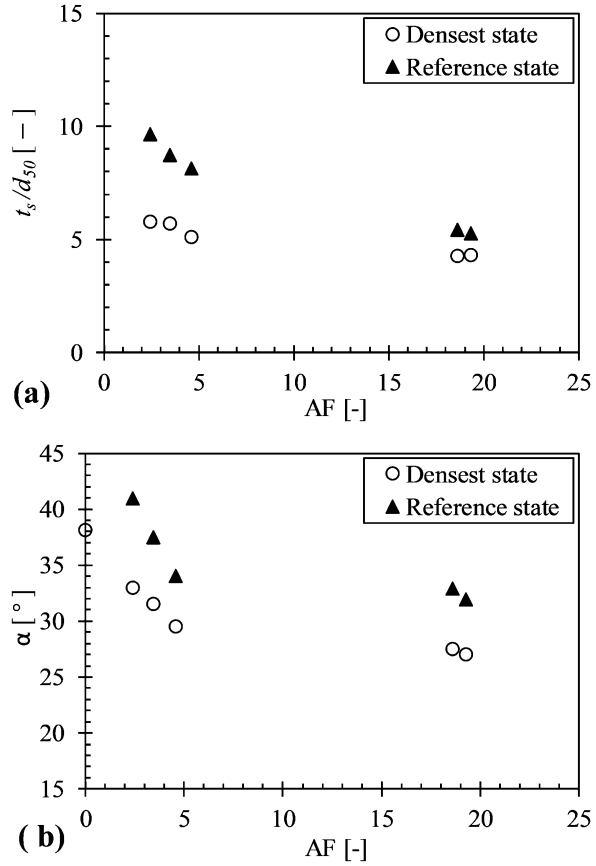


Fig. 13 Dependency of shear band characteristics on particle angularity for passive state a) $t_s / d_{eq}$ -AF b) α - AF

yields the highest $F_{TOTAL}$ magnitude among all simulations (Fig. 14). This is because, the wall must overcome two different forms of resistances; a) the weight of particles inside the failure wedge b) a resistance force that develops due to interlocking, which increases with the increase in *AF*.

The number of particles, and thus the overall mass, varies for backfills with different shaped particles. To be able to observe the influence of granular structure alone, it is necessary to remove the difference caused by density. This is achieved by normalizing the maximum force acting on the retaining wall ($F_{H\ max}$= max ($F_{TOTAL}$)) with the maximum vertical force ($F_{V\ max}$) acting at level of the bottom of the model wall.

The results are plotted with respect to *AF* in Fig. 15. Fig. 15 shows that as *AF* increases, the ratio of $F_{Hmax}/F_{Vmax}$ also increases. The major increase occurs for *AF* values below 5, which might be an indication of the saturation of the *AF* influence, since no major change is seen for AF values above 5.

### 3.2.2 Active state for densely packed models

In this section, the same tests as the previous section are repeated with a wall movement in the opposite direction, ultimately reaching active state. Therefore, granular backfills are identical to the ones used in passive tests with backfills at the densest state.

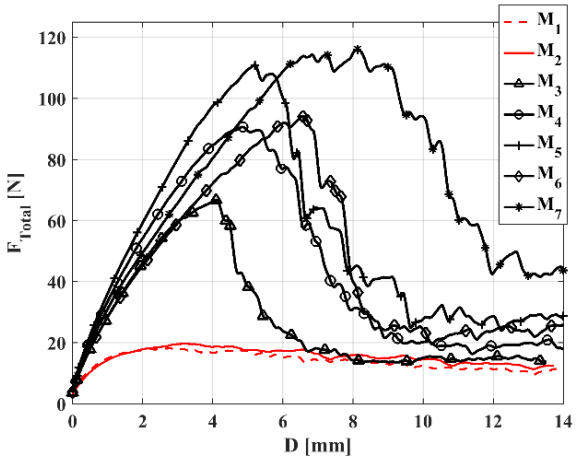


Fig. 14 $F_{TOTAL}$-$D$ relationships for densely packed backfills during model tests towards passive state.

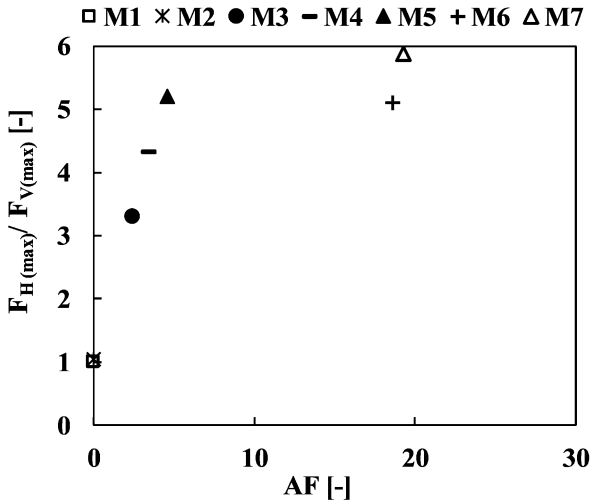


Fig. 15 $F_{Hmax}/F_{Vmax}$ and *AF* correlation for all models tested towards passive state at their densest states.

Accordingly, similar to the passive tests, the distribution of $\theta_i$ is evaluated for differently shaped particles at active failure state, see Fig. 16. Similarly, it is observed that models M1 and M2 present a uniform distribution for $\theta_i$ within the failure wedge (i.e. all the particles inside the failure wedge undergo a similar amount of rotation). For the backfills with non-spherical particles, it is seen that the amount of cumulative rotation is reduced, see Figs. 16-18. Additionally, unlike the passive models with angular particles, it is not possible to identify distinct shear bands in active models.

Repeating the same approach used in passive tests, the distribution of cumulative rotation is determined for active tests. Like the passive case, particles that undergo an insignificant amount of rotation ($\theta_i \leq 0.001$) are excluded from the analyses. Initially, the results of the models with spherical particles (M1 and M2) are compared in Fig. 17. Despite very small differences (i.e. M2 particles present less rotation), the rotational responses are similar. This is in line with the results obtained in passive M1 and M2 models (Fig. 9).

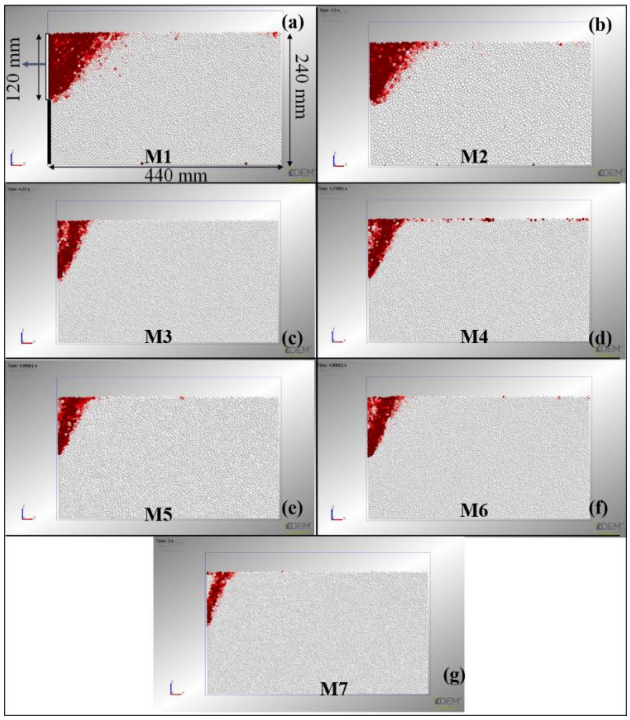


Fig. 16 Distributions of cumulative rotation magnitude ($\theta_i$) for models at the densest state (active tests)

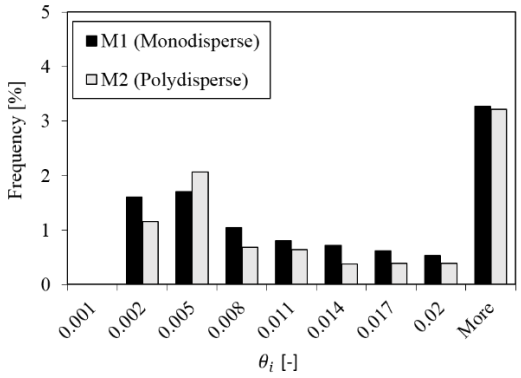


Fig. 17 Comparison of cumulative rotation magnitudes for the particles of M1 and M2 models in active tests with densely packed granular systems (data are obtained at a wall movement of 2 mm)

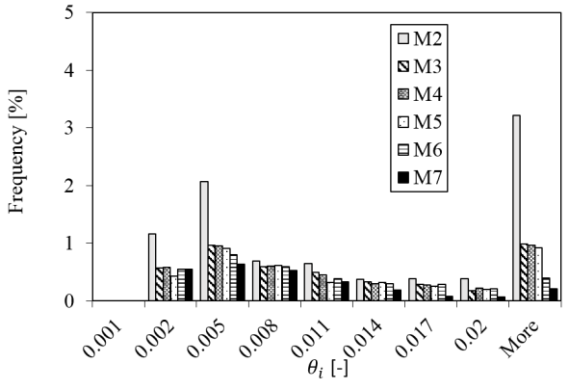


Fig. 18 Comparison of cumulative rotation magnitudes for particles with various angularity factors, active case with initially dense packing (data are obtained at a wall movement of 2 mm)

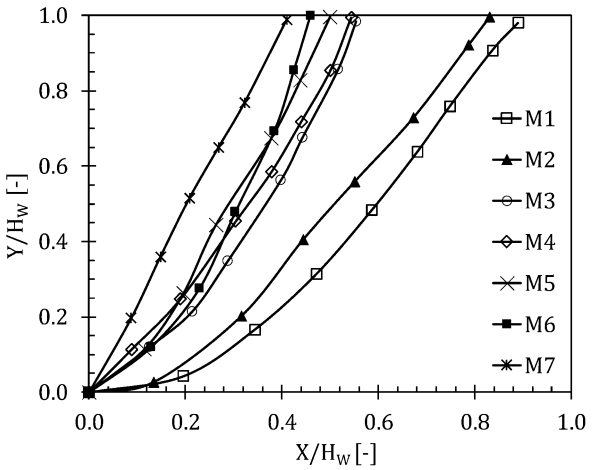


Fig. 19 Active failure surface geometries obtained from models with densely packed particles

Additionally, a quantitative comparison for cumulative rotation distribution is carried out among particles with varied AF (note that since M1 and M2 revealed similar rotational responses, only M2 is presented here), see Fig. 18. Like the passive case, it is observed that the number of rotating particles is bigger for spheres (M2 packing). Moreover, as angularity increases, the frequency of the number of rotating particles, as well as their magnitudes, decreases. Evidently, angularity is an impediment to rotation and for models with more angular particles, shearing concentrates into narrower bands.

Failure surface geometries for all densely packed active models are determined and plotted in Fig. 19. Expectedly, in contrast to passive models, the largest failure wedge is observed for M1, with the close second belonging to M2 model. This order is similar to the results obtained at passive state, an outcome of the increased shearing resistance of polydispersity. For non-spherical particles, it is seen that models composed of particles with higher *AF* produce smaller failure wedges. Different than passive models, geometries of active failure surfaces are not dependent on backfill density. The likely reason for this difference is the much smaller sizes of active failure wedges. Additionally, the weights of backfill confined within active wedges are similar for all models, since the sizes of all active wedges are very close. As a result, it can be suggested that the particle shape influence is stress-path dependent.

Evident in Fig. 20(a), for densely packed active models $t_s$ / $d_{eq}$ reduces slightly with increasing *AF*, suggesting an inverse relationship between particle angularity and shear band thickness. The observed thicknesses at the active state for densely packed models are comparable with those reported by Jiang *et al*. (2014). Soltanbeigi *et al*. (2019) conducted physical model tests simulating active failure problems and showed that shear band thickness is inversely proportional to backfill dilatancy. When the results are shown in Fig. 20(a) are compared with the results given by Soltanbeigi *et al*. (2019), it is noticed that they follow the same trend. This is expected since materials composed of particles with greater AF are more dilatant.

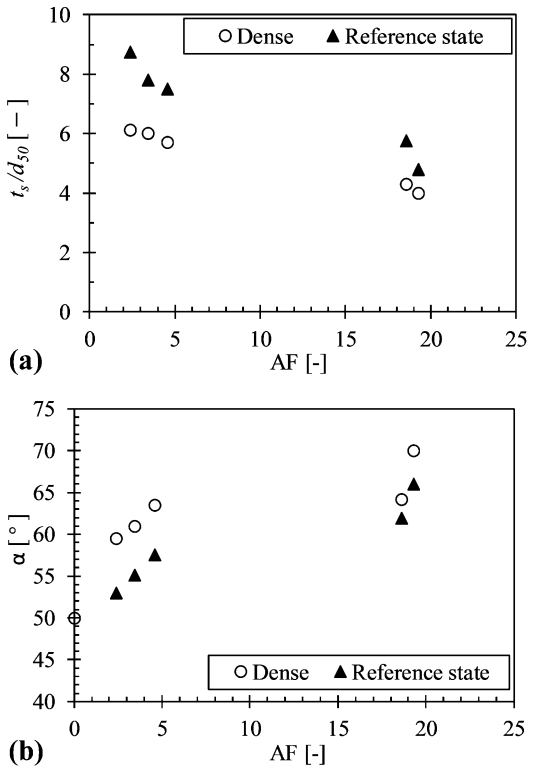


Fig. 20 Dependency of shear band characteristics on particle angularity for active state a) $t_s / d_{eq}$ -AF b) $\alpha$ - AF

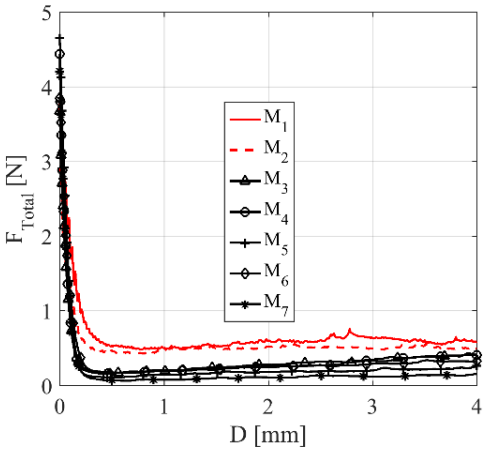


Fig. 21 $F_{TOTAL}$-$D$ relationships for densely packed backfills during model tests towards active state

Meanwhile, the variation of $\alpha$ with $AF$ for densely packed active models is shown in Fig. 20(b) The measured inclinations are comparable with observations of (Jiang *et al*. 2014, Leśniewska *et al*. 2012, Lesniewska and Muir Wood 2011, Niedostatkiewicz *et al*. 2011, Nitka *et al*. 2015, Nübel 2002, Tehrani *et al*. 2014, Widuliński *et al*. 2011).

$F_{TOTAL}$-$D$ relationships for active model tests are presented in Fig. 21. It must be noted that no rolling resistance is utilized in the models presented here. As mechanically expected, models with spherical particles exert higher forces on the retaining wall. Variations of $F_{TOTAL}$ for models with spherical particles (M1 and M2) are almost overlapping, with poly-disperse system exerting slightly less force on the retaining wall.

In case of non-spherical particles, as angularity increases, the total force exerted on the wall decreases (Fig. 21). This is in agreement with the results presented in Fig. 19.

### 3.3 Influence of particle shape for backfills prepared at a reference density

The previous section presents the results of models with backfills prepared at their densest states and examines the influence of grain shape on behaviour for both passive and active modes of wall translations. This way, it is possible to compare the grain shape effect at a natural condition. However, the densest state is also a function of grain morphology and the results are unavoidably affected by the differences in resulting *SF* differences. In this section, to eliminate the impact of *SF* differences on the results, the same study of the previous section will now be repeated with models that are prepared at the same density. The method of preparing backfills at a common density is explained in the "the numerical model" section. At the target reference density, all models' *SF* values are 0.655, which is the average of the *SF* values of M1 and M2 models at their densest states. Accordingly, the simulations in this section only consider M3, M4, M5, M6 and M7 particles.

#### 3.3.1 Passive state at a reference density

Following the same approach used with the dense models, magnitudes and spatial distributions of cumulative rotations for the models prepared at the reference density are determined. These are presented in Fig. 22. The results of M1 and M2 models are the same as those obtained in the previous section, because their density is used as the reference density in this section. That is why, cumulative rotation distributions of M1 and M2 models are not shown in Fig. 22, as they are available in Fig. 8.

When Fig. 22 is examined, it is noticed that the results of M3 and M4 are significantly different than their results with dense models (Fig. 8). In Fig. 22, particle rotation is not strictly concentrated within a specific region along with the shear band and the resulting shear bands are thicker. This is an outcome of the differences between densities. Considering the change in stresses to be insignificant, these granular systems will have smaller friction and dilatancy angles (Bolton 1986, Cinicioglu and Abadkon 2015). Soltanbeigi *et al.* (2019) experimentally showed that shear band thickness is directly dependent on peak dilation angle and the results of DEM models confirm this observation.

Similarly, for backfills with more angular particles (M5, M6 and M7), the intensities of particle rotation along the shear bands (Fig. 22) are less than they are in the dense models (Fig. 8). This is because these models are now in a looser state and therefore particle interlocking is less intense and the produced shear bands are wider and less distinct (compared to denser backfills). An increase in the thickness of a shear band lessens the extent of required particle rotation, since shear deformations are distributed to a wider area. This is in line with the observations of (Soltanbeigi *et al*. 2019). In any case, it is important to note that models with more angular particles produce more distinct shear bands, as evidenced in Fig. 22.

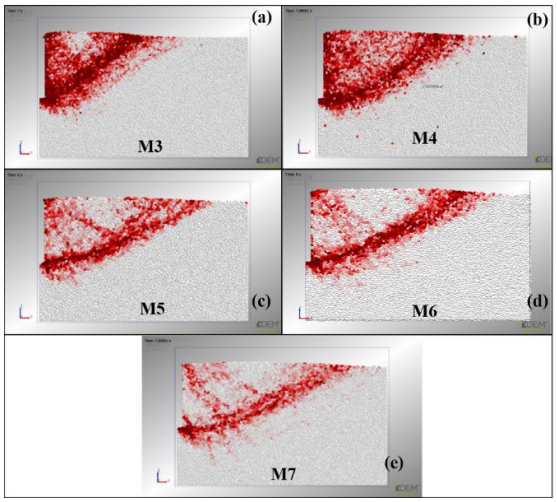


Fig. 22 Distribution of cumulative rotation magnitude ($\theta_i$) for each model at the reference density in passive simulations

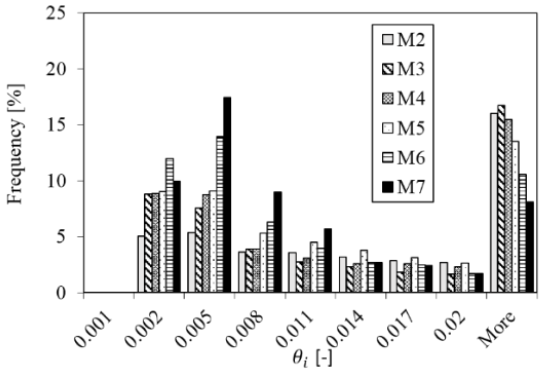


Fig. 23 Comparison of cumulative rotation magnitudes for particles with various angularity factors, passive case with models prepared at the reference density (data are obtained at the steady-state)

Fig. 23 presents the quantitative comparison of cumulative rotation magnitudes for all passive tests at the reference density (M1 is not included as its results are the same as M2). As angularity increases at the same density, the number of particles that experience a significant amount of rotation decreases. This is a consequence of the confinement of shearing into a narrower zone for more angular particles. Thinner shear bands that emerge in models with more angular particles naturally limit the number of particles that go through large amounts of rotations.

Fig. 24 presents the failure surfaces of all passive models at the reference density. Obviously, when all models are at the same density, ones with more angular particles produce larger passive failure wedges. This is because when all models are at the same density and approximately same stress state, assemblies with more angular particles have greater friction angles.

Geometrical characteristics such as thickness and inclination are also considered for failure surfaces shown in Fig. 22. Accordingly, $t_s$ / $d_{eq}$ – $AF$ and $\alpha$– $AF$ for these models are shown in Fig. 13, respectively. The overall

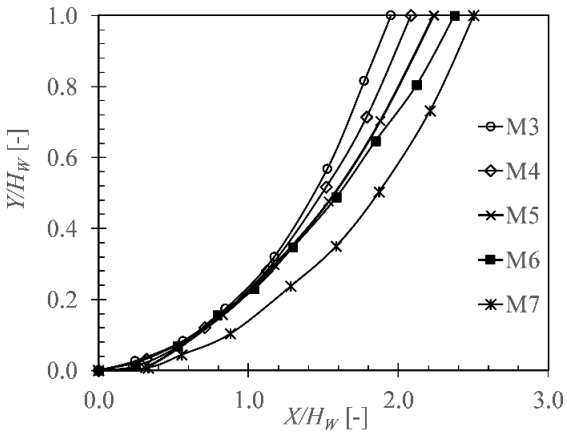


Fig. 24 Failure surface geometries for models at the reference density (passive state)

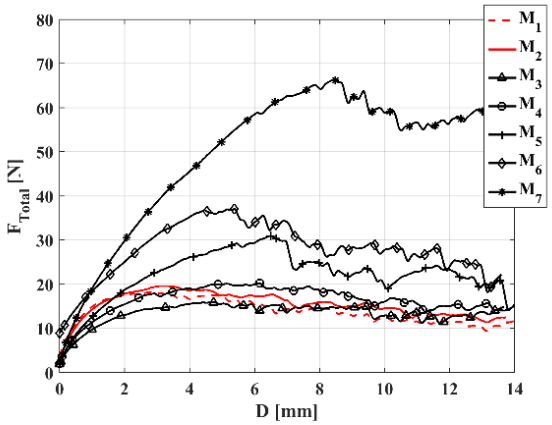


Fig. 25 $F_{TOTAL}$-$D$ relationships obtained in passive model tests with backfills prepared at the reference density

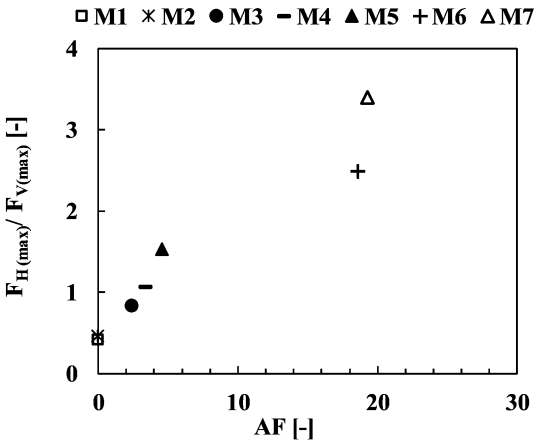


Fig. 26 $F_{Hmax}/F_{Vmax}$ and $AF$ correlation for all models tested towards passive state with backfills prepared at the reference density

trends are similar to those of dense backfills with the differences in magnitudes owing to the differences in backfill densities. Backfills at reference density yield thicker and steeper shear bands.

Variation $F_{TOTAL}$ with $D$ is shown for all models at the reference density are shown in Fig. 25. It is seen that

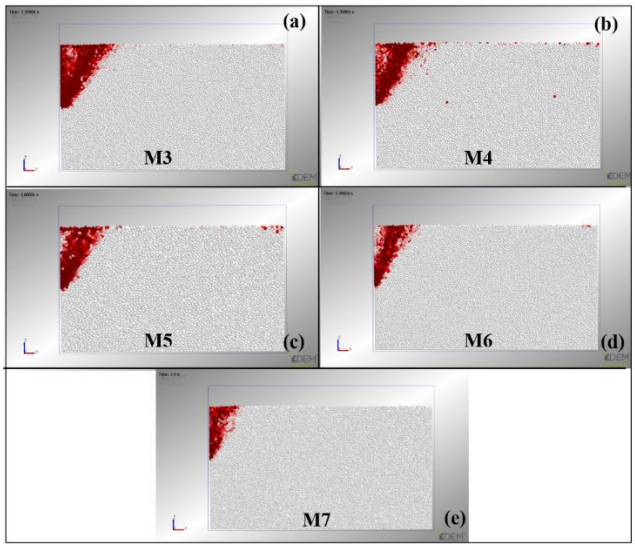


Fig. 27 Distribution of cumulative rotation magnitude ($\theta_i$) for models at the reference density (active tests)

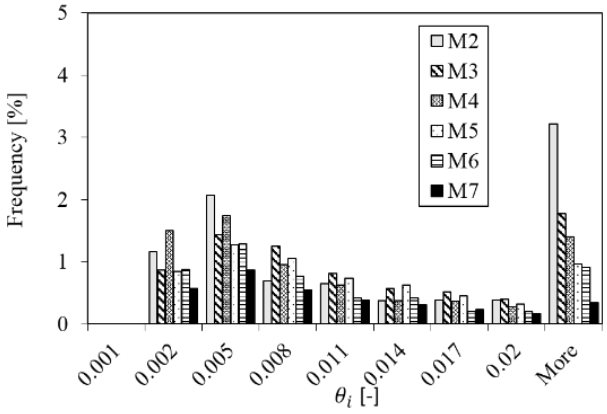


Fig. 28 Comparison of cumulative rotation magnitudes for particles with various angularity factors, active case with backfill at the reference density (data are obtained at a wall movement of 2 mm)

$F_{TOTAL}$-$D$ relationships of models M1, M2, M3, and M4 are very close to each other. These models directly shear to steady-state deformation without a peak. The density state of these backfills is then considered loose, following the convention in soil mechanics (Wood 1990). Among these four models, backfills of M3 and M4 are not prepared at their possible maximum density; their responses are loose. Yet, the backfills of models M1 and M2 are at their densest states. But their response lacks a peak and therefore is considered a loose response. This is a consequence of using spherical particles. In the absence of angularity, it is not possible to capture peak response observed with granular arrangements that are considered dense in the context of soil mechanics. On the other hand, $F_{TOTAL}$-$D$ relationships of models M5, M6, and M7 have peaks indicating "denser" response in the sense of soil mechanics. Evident in Fig. 25, the magnitudes of $F_{TOTAL}$ in these tests are increasing with the increases in their respective $AF$ values. Therefore, it is possible to propose that particle angularity enhances interlocking even in loose backfills.

The dependency of the total force on angularity is considered in Fig. 26. For this purpose, the maximum force acting on the retaining wall ($F_{H\ max}$) is normalized by the maximum vertical force ($F_{V\ max}$) that acts at the level of the bottom of the model wall. The magnitudes of $F_{Hmax}/F_{Vmax}$ versus $AF$ for passive model simulations at the reference density are shown in Fig. 26. The results suggest that at reference density, the particle angularity clearly plays a direct role in both failure surface geometry and force exerted on the wall.

### 3.3.2 Active state at a reference density

Model simulations with backfills prepared at the reference density are repeated for wall movements towards the active state.

The spatial distribution of cumulative rotation is presented for all active tests with angular particles are shown in Fig. 27. Results for models with spherical particles (M1 and M2 models) are not repeated here, since they are the same as those presented in Fig. 16. Comparing the results in Fig. 27 and Fig. 16 visually, it seems as if density does not have an impact on the magnitude and distribution of $\theta_i$ for active cases. However, this is caused by the difficulty in visually distinguishing differences when the results of all models are confined to a narrow zone. Therefore, the results should be interpreted using the data in Fig. 28. When the magnitudes of cumulative rotations and their frequencies for different rotation magnitudes (Fig. 28) are compared with the results in dense models (Fig. 18), it is clear that the number of particles that rotate notably decreased. This is a common observation of both passive and active tests. Whenever a model is denser, deformations concentrate within a narrower zone and as a result, smaller number of particles participate in the shearing process. In case of models composed of angular particles, more angular particles cause deformations to take place within an even narrower area, reducing the frequency of particles that experience significant rotation, as evidenced by the results in Fig. 28.

Fig. 29 presents the geometries of active failure planes determined for tests at the reference density. This is in line with the expected mechanical response because more angular particles correspond to greater internal friction angles.

Variations of thicknesses and inclinations of shear bands in Fig. 27 are quantified in Figs. 20(a)-(b), respectively. Apparently, the general trends for $t_s / d_{eq} - AF$ and $\alpha - AF$ are similar to those of dense backfills. The differences in magnitudes are due to the differences in backfill densities. Manifestly, backfills at reference density yield thicker but less steep shear bands. This is in congruence with the expected mechanical response according to which active shear bands become thinner and steeper at greater relative densities.

Additionally, it is obvious in Fig. 30 that as AF increases, total force exerted on the wall at the active state decreases; this is the expected response from smaller wedges. Moreover, similar to the results in the passive tests with models at the reference density, models M3 and M4 exert similar total forces as do models with spherical

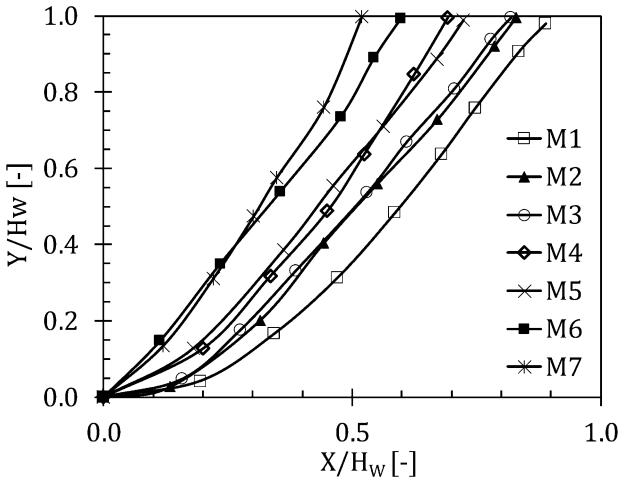


Fig. 29 Active failure surface geometries obtained from models with backfills prepared at the reference density

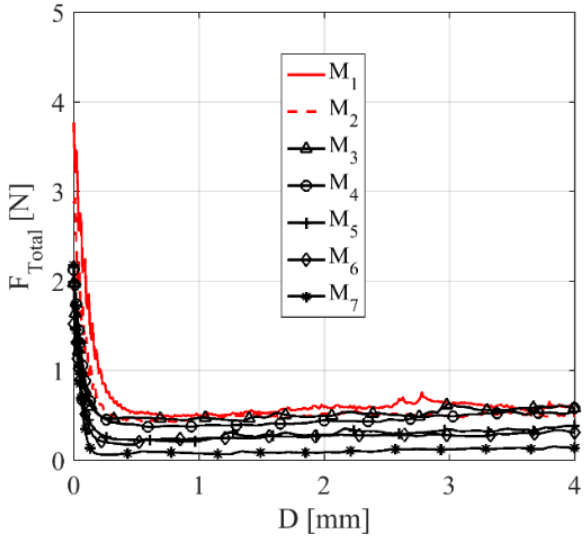


Fig. 30 $F_{TOTAL}$-$D$ relationships of active model tests with backfills prepared at the reference density

particles (M1 and M2). As explained in the section on passive tests, models M3 and M4 show "loose" response at the reference density and as a result their active thrusts are similar to the active thrust of models with spherical particles.

## 4. Conclusions

In this study, the influences of particle shape on the response of retained granular backfills are investigated. For this purpose, DEM models are prepared at various densities and are subjected to two different stress paths. The aim is twofold; understanding the mechanics underlying the influence particle shape on behaviour, and to shed light on the effects of possible DEM modelling choices. Accordingly, a comparative modelling program is planned, which would allow assessing the suitability of using a certain rolling resistance (i.e. Type D) as a substitute for shape factor and determining the relative contributions of different backfill characteristics on retained soil response. Two stress paths are followed culminating in either of the two geotechnical failure modes for retaining structures; active and passive deformations. Consequently, for the observed shear bands, the influences of particle shape on bands' geometrical characteristics are examined with this study.

The main results of the study are summarized here:

- The default rolling resistance model of EDEM is not suitable for modelling retained backfills, since the incorporated torque calculation method is inadequate.
- Shear band characteristics such as its position with respect to the wall, its thickness, and inclination are controlled by the combined influences of stress path, density state and particle shape.
- For spherical particles, irrespective of density, there is no clear shear banding and all particles within the failure wedge participate in deformation.
- Regarding gradation, the following observations are obtained for assemblies with spherical particles:

  - Particles in poly-disperse assemblies experience less rotation, since each particle has a bigger number of contacts and particles have less freedom to rotate.

  - Polydispersity has marginal influence over failure surface geometry.
- When all else is constant, increasing particle angularity leads to:

  - Thinner shear bands in both passive and active cases. The thicknesses range between 4 $d_{eq}$ to 9 $d_{eq}$ for both.

  - Greater shear band inclinations for active case (50°-70°); for passive problems, vice versa (27°-41°).

  - Greater shear band inclinations for active problems; for passive problems, vice versa.
- For backfills with the same density; the backfill composed of more angular particles will have a smaller number of grains experiencing a significant amount of rotation, but for these grains, the intensity of rotation will be greater. Rounder particles produce wider bands of shearing; wider shear bands lessen the extent of required particle rotation, since shear deformations are distributed over the failure wedge.
- Even at the densest possible state, responses of backfills composed of spherical particles are loose (i.e. not have a peak response in $F_{TOTAL}$ - $D$) according to soil mechanics convention.
- When all parameters are the same, angular particles lead to looser backfills.
- Overall, particle shape and packing density have coupled influences over failure surface geometry of densely packed granular assemblies. However, density exerts much greater influence over failure surface geometry; accordingly, the size of passive wedge is a linear function of solid fraction for backfills prepared at the densest state.

As a final note, the models in this study are composed of particles that only overlap but do not break. For retained backfills, stress levels are low and therefore particle crushing is rare. However, it is important to consider particle crushing and the resulting changes in grain shape and gradation for backfills made up of crushable (i.e., calcareous) sands.

## Acknowledgments

The authors would like to thank The Scientific and Research Council of Turkey (TÜBITAK) for supporting this study with Project number 114M329.

## References

Ai, J., Chen, J.F., Rotter, J.M. and Ooi, J.Y. (2011), "Assessment of rolling resistance models in discrete element simulations", *Powder Technol.*, **206**(3), 269-282. https://doi.org/10.1016/j.powtec.2010.09.030.

Alshibli, K.A. and Cil, M.B. (2018), "Influence of particle morphology on the friction and dilatancy of sand", *J. Geotech. Geoenvironmental Eng.*, **144**(3), 4017118. https://doi.org/10.1061/(ASCE)GT.1943-5606.0001841.

Altunbas, A., Soltanbeigi, B. and Cinicioglu, O. (2017), "Determination of active failure surface geometry for cohesionless backfills", *Geomech. Eng.*, **12**(6), 983-1001. https://doi.org/10.12989/gae.2017.12.6.983.

Altunbas, A., Soltanbeigi, B. and Cinicioglu, O. (2019), "DEM analysis of passive failure state behind a rigid retaining wall: Effect of boundary conditions", *IS-Glasgow 2019–7th International Symposium on Deformation Characteristics of Geomaterials*, Glasgow, June. https://doi.org/10.1051/e3sconf/20199214012.

Bardet, J.P. and Huang, Q. (1992), "Numerical modeling of micropolar effects in idealized granular materials", *Mech. Granul. Mater. Powder Syst.*, **37**, 85-91.

Bolton, M.D. (1986), "The strength and dilatancy of sands", *Geotechnique*, **36**(1), 65-78. https://doi.org/10.1680/geot.1986.36.1.65.

Bono, J.P. de and McDowell, G.R. (2014), "DEM of triaxial tests on crushable sand", *Granul. Matter*, **16**(4), 551-562. https://doi.org/10.1007/s10035-014-0500-x.

Cho, G.C., Dodds, J. and Santamarina, J.C. (2006), "Particle shape effects on packing density, stiffness and strength: Natural and crushed sands", *J. Geotech. Geoenvironmental Eng.*, **132**(5), 591-602. https://doi.org/10.1061/(ASCE)1090-0241(2006)132:5(591).

Cinicioglu, O. and Abadkon, A. (2015), "Dilatancy and friction angles based on in situ soil conditions", *J. Geotech. Geoenvironmental Eng.*, **141**(4), 6014019. https://doi.org/10.1061/(ASCE)GT.1943-5606.0001272.

Coulomb, C.A. (1776), "An attempt to apply the rules of maxima and minima to several problems of stability related to architecture", *Mémoires l'Académie R. Des Sci.*, **7**, 343-382.

Cundall, P.A. and Strack, O.D.L. (1979), "A discrete numerical model for granular assemblies", *Geotechnique*, **29**(1), 47-65. https://doi.org/10.1680/geot.1979.29.1.47.

Gezgin, A.T. and Cinicioglu, O. (2019), "Consideration of locked-in stresses during backfill preparation", *Geomech. Eng.*, **18**(3), 247-258. https://doi.org/10.12989/gae.2019.18.3.247.

Gezgin, A.T., Soltanbeigi, B. and Cinicioglu, O. (2020), "Discrete-element modelling of pile penetration to reveal influence of soil characteristics", *Proc. Inst. Civil Engineers-Geotech. Eng.*, **2020**, 1-42. https://doi.org/10.1680/jgeen.20.00134.

Gezgin, A.T., Soltanbeigi, B., Altunbas, A. and Cinicioglu, O. (2021), "Multi-scale investigation of active failure for various modes of wall movement", *Front. Struct. Civ. Eng.* **15,** 961-979. https://doi.org/10.1007/s11709-021-0738-4.

Hanna, A. and Al Khoury, I. (2005), "Passive earth pressure of overconsolidated cohesionless backfill", *J. Geotech. Geoenviron. Eng.*, **131**(8), 978-986. https://doi.org/10.1061/(ASCE)1090-0241(2005)131:8(978).

Holtz, R.D., Kovacs, W.D. and Sheahan, T.C. (1981), *An Introduction to Geotechnical Engineering, Vol. 733*, Prentice-Hall, NJ, USA.

Holubec, I. and D'appolonia, E. (1973), "Effect of particle shape on the engineering properties of granular soils", *Evaluation of Relative Density and Its Role in Geotechnical Projects Involving Cohesionless Soils*, 304-318, ASTM International, PA, USA.

Iwashita, K. and Oda, M. (1998), "Rolling resistance at contacts in simulation of shear band development by DEM", *J. Eng. Mech.*, **124**(3), 285-292. https://doi.org/10.1061/(ASCE)0733-9399(1998)124:3(285).

Jiang, M., He, J., Wang, J., Liu, F. and Zhang, W. (2014), "Distinct simulation of earth pressure against a rigid retaining wall considering inter-particle rolling resistance in sandy backfill", *Granul. Matter*, **16**(5), 797-814. https://doi.org/10.1007/s10035-014-0515-3.

Jiang, M.J., Yu, H.S. and Harris, D. (2005), "A novel discrete model for granular material incorporating rolling resistance", *Comput. Geotech.*, **32**(5), 340-357. https://doi.org/10.1016/j.compgeo.2005.05.001

Kamiloglu, H.A. and Sadoglu, E. (2019), "Experimental and theoretical investigation of short-and long-heel cases of cantilever retaining walls in active state", *Int. J. Geomech.*, **19**(5), 4019023. https://doi.org/10.12989/gae.2013.5.6.499

Keshavarz, A. and Pooresmaeil, Z. (2016), "Static and seismic active lateral earth pressure coefficients for c-ϕ soils", *Geomech. Eng.*, **10**(5), 657-676. https://doi.org/10.12989/gae.2016.10.5.657.

Khosravi, M.H., Hamedi Azad, F., Bahaaddini, M. and Pipatpongsa, T. (2017), "DEM Analysis of Backfilled Walls Subjected to Active Translation Mode", *Int. J. Min. Geo-Engineering*, **51**(2), 191-197. https://dx.doi.org/10.22059/ijmge.2017.233613.594675.

Lee, S.W. (2019), "Experimental study on effect of underground excavation distance on the behavior of retaining wall", *Geomech. Eng.*, **17**(5), 413-420. https://doi.org/10.12989/gae.2019.17.5.413.

Lesniewska, D. and Muir Wood, D. (2011), "Photoelastic and photographic study of a granular material", *Geotechnique*, **61**(7), 605-611. https://doi.org/10.1680/geot.8.T.017.

Leśniewska, D., Niedostatkiewicz, M. and Tejchman, J. (2012), "Experimental study on shear localisation in granular materials within combined strain and stress field", *Strain*, **48**(5), 430-444. https://doi.org/10.1111/j.1475-1305.2012.00838.x.

Lim, M.S., Wijeyesekera, D.C., Zainorabidin, A. and Bakar, I. (2012), "The effects of particle morphology (shape and sizes) characteristics on its engineering behaviour and sustainable engineering performance of sand", *Int. J. Integr. Eng.*, **4**(3), 27-37.

Nadukuru, S.S. and Michalowski, R.L. (2012), "Arching in distribution of active load on retaining walls", *J. Geotech. Geoenvironmental Eng.*, **138**(5), 575-584. https://doi.org/10.1061/(ASCE)GT.1943-5606.0000617.

Niedostatkiewicz, M., Lesniewska, D. and Tejchman, J. (2011), "Experimental analysis of shear zone patterns in cohesionless for earth pressure problems using particle image velocimetry", *Strain*, **47**(SUPPL. 2), 218-231. https://doi.org/10.1111/j.1475-1305.2010.00761.x.

Nitka, M., Tejchman, J., Kozicki, J. and Leśniewska, D. (2015), "DEM analysis of micro-structural events within granular shear zones under passive earth pressure conditions", *Granul. Matter*, **17**(3), 325-343. https://doi.org/10.1007/s10035-015-0558-0.

Nübel, K. (2002), *Experimental and Numerical Investigation of Shear Localization in Granular Material*, TIB Hannover, Germany.

O'Sullivan, C. (2011), *Particulate Discrete Element Modelling: A Geomechanics Perspective,* CRC Press, Florida, USA.

Oda, M. and Kazama, H. (1998), "Microstructure of shear bands and its relation to the mechanisms of dilatancy and failure of dense granular soils", *Geotechnique*, **48**(4), 465-481.

https://doi.org/10.1680/geot.1998.48.4.465

Rankine, W.J.M. (1857), "II. On the stability of loose earth", *Philosopical Transactions*, 9-27, The Royal Society, London, United Kingdom.

Rechenmacher, A.L., Abedi, S., Chupin, O. and Orlando, A.D. (2011), "Characterization of mesoscale instabilities in localized granular shear using digital image correlation", *Acta Geotech.*, **6**(4), 205-217. https://doi.org/10.1007/s11440-011-0147-2.

Rodriguez, J. M., Edeskär, T. and Knutsson, S. (2013), "Particle shape quantities and measurement techniques-A review", *Electron. J. Geotech. Eng.*, **18**, 169-198.

Sakaguchi, H., Ozaki, E. and Igarashi, T. (1993), "Plugging of the flow of granular materials during the discharge from a silo", *Int. J. Mod. Phys. B*, **7**(09n10), 1949-1963. https://doi.org/10.1142/S0217979293002705.

Sancak, E. and Cinicioglu, O. (2020), "Selection of design friction angle : A strain based empirical method for coarse grained soils", *Geomech. Eng.*, **20**(2), 121-129. https://doi.org/10.12989/gae.2020.20.2.121.

Shin, H. and Santamarina, J.C. (2013), "Role of particle angularity on the mechanical behavior of granular mixtures", *J. Geotech. Geoenvironmental Eng.*, **139**(2), 353-355. https://doi.org/10.1061/(ASCE)GT.1943-5606.0000768.

Soltanbeigi, B. (2019), "Multi-scale analysis of the influence of particle shape on the mechanical response of granular materials", Ph.D. Dissertation, The University of Edinburgh, Edinburgh. https://era.ed.ac.uk/handle/1842/35752.

Soltanbeigi, B., Altunbas, A. and Cinicioglu, O. (2019), "Influence of dilatancy on shear band characteristics of granular backfills", *Eur. J. Environ. Civ. Eng.*, 1-18. https://doi.org/10.1080/19648189.2019.1572542

Soltanbeigi, B., Altunbas, A., Gezgin, A.T. and Cinicioglu, O. (2020), "Determination of passive failure surface geometry for cohesionless backfills", *Periodica Polytech. Civil Eng.*, **64**(4), 1100-1110. https://doi.org/10.3311/PPci.14241.

Soltanbeigi, B., Papanicolopulos, S. and Ooi, J.Y. (2016), "Particle shape effect on deformation localization during quasi-static flow at active state", *5th International Conference on Geotechnical Engineering and Soil Mechanics*, Tehran, November.

Soltanbeigi, B., Podlozhnyuk, A., Papanicolopulos, S. A., Kloss, C., Pirker, S. and Ooi, J. Y. (2018), "DEM study of mechanical characteristics of multi-spherical and superquadric particles at micro and macro scales", *Powder Technol.*, **329**, 288-303. https://doi.org/10.1016/j.powtec.2018.01.082.

Sukumaran, B. and Ashmawy, A.K. (2001), "Quantitative characterisation of the geometry of discrete particles", *Geotechnique*, **51**(7), 619-627. https://doi.org/10.1680/geot.2001.51.7.619.

Tang, H., Dong, Y., Chu, X. and Zhang, X. (2016), "The influence of particle rolling and imperfections on the formation of shear bands in granular material", *Granul. Matter*, **18**(1), 12. https://doi.org/10.1007/s10035-016-0607-3.

Tehrani, F.S., Arshad, M.I., Prezzi, M. and Salgado, R. (2014), "Visualization of active mode of failure behind flexible walls under pure rotation using digital image correlation", *Geo-Congress 2014 Geo-Characterization Modeling Sustainability*, 3393-3402, Atlanta, February.

Tejchman, J., Bauer, E. and Tantono, S.F. (2007), "Influence of initial density of cohesionless soil on evolution of passive earth pressure", *Acta Geotech.*, **2**(1), 53-63. https://doi.org/10.1007/s11440-007-0022-3.

Terzaghi, K. (1943), *Theoretical Soil Mechanics,* John Wiley and Sons, NJ, USA.

Tian, J., Liu, E. and He, C. (2020), "Shear band analysis of granular materials considering effects of particle shape", *Acta Mech.*, **231**(11), 4445-4461. https://doi.org/https://doi.org/10.1007/s00707-020-02771-y.

Toyosawa, Y., Itoh, K., Tamrakar, S.B. and Suemasa, N. (2006), "Redistribution of active earth pressures using movable earth support apparatus in centrifuge", *Proceedings of 6th International Conference on Physical Modelling in Geotechnics*, **2**(4), 1113-1118. https://doi.org/10.1201/noe0415415866.ch163.

Vangla, P. and Latha, G.M. (2015), "Influence of particle size on the friction and interfacial shear strength of sands of similar morphology", *Int. J. Geosynth. Gr. Eng.*, **1**(1), 6. https://doi.org/10.1007/s40891-014-0008-9.

Wiącek, J. and Molenda, M. (2014), "Effect of particle size distribution on micro-and macromechanical response of granular packings under compression", *Int. J. Solids Struct.*, **51**(25-26), 4189-4195. https://doi.org/10.1016/j.ijsolstr.2014.06.029.

Widuliński, Ł., Tejchman, J., Kozicki, J. and Leśniewska, D. (2011), "Discrete simulations of shear zone patterning in sand in earth pressure problems of a retaining wall", *J. Solids Struct.*, **48**(7), 1191-1209. https://doi.org/https://doi.org/10.1016/j.ijsolstr.2011.01.005.

Wood, D.M. (1990), *Soil Behaviour and Critical State Soil Mechanics,* Cambridge University Press, Cambridge, United Kingdom.

Zhao, S., Evans, T. M. and Zhou, X. (2017), "Random packing of tetrahedral particles using the polyhedral and multi-sphere discrete element method", *Springer Proc. Phys.*, **188**, 91-99. https://doi.org/10.1007/978-981-10-1926-5_11.

Zheng, D.F., Nian, T.K., Liu, B., Yin, P. and Song, L. (2015), "Coefficient charts for active earth pressures under combined loadings", *Geomech. Eng.*, **8**(3), 461-476. https://doi.org/10.12989/gae.2015.8.3.461.

Zhou, Y.C., Wright, B.D., Yang, R. Y., Xu, B. H. and Yu, A.B. (1999), "Rolling friction in the dynamic simulation of sandpile formation", *Phys. A Stat. Mech. Its Appl.*, **269**(2-4), 536-553. https://doi.org/10.1016/S0378-4371(99)00183-1.

Zhuang, L., Nakata, Y. and Lee, I.M. (2013), "Localized deformation in sands and glass beads subjected to plane strain compressions", *Geomech. Eng.*, **5**(6), 499-517. https://doi.org/10.12989/gae.2013.5.6.499.

Zhuang, L., Nakata, Y., Kim, U.G. and Kim, D. (2014), "Influence of relative density, particle shape and stress path on the plane strain compression behavior of granular materials", *Acta Geotech.*, **9**(2), 241-255. https://doi.org/10.1007/s11440-013-0253-4.

*CC*